EPJ manuscript No.
(will be inserted by the editor)

Spin assignments for ^{23}Mg levels and the astrophysical ^{22}Na(p,γ)^{23}Mg reaction

M.S. Kwag[1], K.Y. Chae[1,a], S. Ahn[2], D.W. Bardayan[3], K.A. Chipps[4], J.A. Cizewski[5], M.E. Howard[5], R.L. Kozub[6], K. Kwak[7], B. Manning[5], M. Matos[8], P.D. O'Malley[5], S.D. Pain[9], W.A. Peters[10], S.T. Pittman[9], A. Ratkiewicz[5], M.S. Smith[9], and S. Strauss[5]

[1] Department of Physics, Sungkyunkwan University, Suwon 16149, Korea
[2] Department of Physics and Astronomy, University of Tennessee, Knoxville, Tennessee 37996, USA
[3] Department of Physics, University of Notre Dame, Notre Dame, Indiana 46556, USA
[4] Department of Physics, Colorado School of Mines, Golden, Colorado 80401, USA
[5] Department of Physics and Astronomy, Rutgers University, New Brunswick, New Jersey 08903, USA
[6] Department of Physics, Tennessee Technological University, Cookeville, Tennessee 38505, USA
[7] School of Natural Science, Ulsan National Institute of Science and Technology (UNIST), Ulsan 44919, Korea
[8] Department of Physics and Astronomy, Louisiana State University, Baton Rouge, LA 70803, USA
[9] Physics Division, Oak Ridge National Laboratory, Oak Ridge, Tennessee 37831, USA
[10] Oak Ridge Associated Universities, Oak Ridge, Tennessee 37831, USA

Received: date / Revised version: date

Abstract. The ^{22}Na(p,γ)^{23}Mg reaction is responsible for destruction of the long-lived radionuclide ^{22}Na produced during nova explosions. Since the reaction proceeds through resonances from levels in ^{23}Mg above the proton threshold at 7.581 MeV, the properties of these levels such as excitation energies, spins, and parities are crucial ingredients to determine the ^{22}Na(p,γ)^{23}Mg reaction rate. Despite recent studies of these levels, their spins are not well constrained in many cases. We have measured the ^{24}Mg(p,d)^{23}Mg transfer reaction to determine spectroscopic properties of these levels at the Holifield Radioactive Ion Beam Facility at Oak Ridge National Laboratory. The spin of the E_x = 7.788 MeV level in ^{23}Mg is constrained to be $J^\pi = (3/2^+, 5/2^+)$ through the present work. The astrophysical ^{22}Na(p,γ)^{23}Mg reaction rate at nova temperatures is updated accordingly. Nova nucleosynthesis model calculations using the newly updated ^{22}Na(p,γ)^{23}Mg reaction rate shows that the final weighted abundance of the radionuclide ^{22}Na is increased by 42% compared to that obtained by using the previous ^{22}Na(p,γ)^{23}Mg reaction rate of Sallaska *et al.* for a 1.35 $M_\odot$ ONeMg white dwarf.

PACS. 26.30.-k – 25.70.Hi – 27.30.+t – 21.10.Hw

1 Introduction

The 1.275 MeV γ-ray originating from the β-decay of the long-lived radionuclide ^{22}Na is a target of the International Gamma-Ray Astrophysics Laboratory (INTEGRAL) launched by the European Space Agency (ESA) [1,2] and the future missions with advanced spectroscopy such as Advanced Compton Telescope (ACT) [3] and enhanced ASTROGAM (e-ASTROGAM) [4]. Owing to the relatively long half-life of ^{22}Na ($t_{1/2}$ = 2.602 yr), it is believed that ^{22}Na lives for a long enough time from its production in a nova outburst until the ejected material becomes transparent to γ-rays [5]. As a result, it is possible to observe the 1.275 MeV γ-ray across the Galaxy. Observations of galactic 1.275 MeV γ-rays therefore provide a critical constraint on the nucleosynthesis occurring in nova explosions if the relevant nuclear reactions are understood.

During nova explosions, ^{22}Na can be synthesized either by proton capture on ^{21}Ne or by β^+-decay of ^{22}Mg [6]. The ^{22}Na(p,γ)^{23}Mg thermonuclear fusion reaction is believed to dominate the destruction of ^{22}Na [6–8]. Since the reaction proceeds through resonances in the ^{22}Na + p (^{23}Mg) system above the proton threshold located at 7580.97 ± 0.23 keV [9], the properties of the levels in ^{23}Mg above this threshold determine the ^{22}Na(p,γ)^{23}Mg reaction rate at nova temperatures. Because of its importance, the reaction has been studied directly three times by using proton beams and ^{22}Na implanted targets [2,10,11]. These studies have substantially improved our understanding of the energy levels in ^{23}Mg. There are, however, many remaining questions, such as the resonance strengths of a number of critical levels. The E_r = 204 keV (E_x = 7.788 MeV) level is believed to be one of the most important

[a] e-mail: kchae@skku.edu, Fax: +82-31-290-7055

resonances for the astrophysical ^{22}Na(p,γ)^{23}Mg reaction rate at nova temperatures [2,11]. The contributions from 11 resonances, which range from E_r = 43 keV to E_r = 743 keV, were investigated in Ref. [2]. The authors concluded that the contributions from other resonances are negligible compared to that from the 204 keV level. They also found that the contribution from the 275 keV level becomes significant at temperatures $\gtrsim$ 0.4 GK [2]. The resonance strength of the 204 keV level was first measured to be $\omega\gamma$ = 1.8 ± 0.7 meV by Stegmüller *et al.* [11], but more recent work by Sallaska *et al.* [2] showed that the resonance strength is stronger by a factor of more than 3 ($\omega\gamma = 5.7\ ^{+1.6}_{-0.9}$ meV). Due to this discrepancy, the ^{22}Na(p,γ)^{23}Mg reaction rate has a significant uncertainty that makes precise comparison of predictions to ^{22}Na observational upper limits [12] extremely challenging.

The levels in ^{23}Mg also have been investigated many times through various transfer reaction measurements such as ^{24}Mg(^{3}He,α)^{23}Mg [13], ^{25}Mg(p,t)^{23}Mg [14], ^{22}Na(^{3}He,d)^{23}Mg [15], and ^{24}Mg(p,d)^{23}Mg [16–19]. Despite the numerous studies, many spins and parities of ^{23}Mg energy levels above the proton threshold are not well determined, and therefore, there remain significant uncertainties in the ^{22}Na(p,γ)^{23}Mg reaction rate at nova temperatures. To improve our knowledge on this capture reaction rate, we have studied the ^{24}Mg(p,d)^{23}Mg reaction to constrain the spins of ^{23}Mg levels. Although the spin values constrained from present work do not affect the results obtained from direct measurements, the spectroscopic information impacts the ^{22}Na(p,γ)^{23}Mg reaction rate deduced from previous indirect measurements.

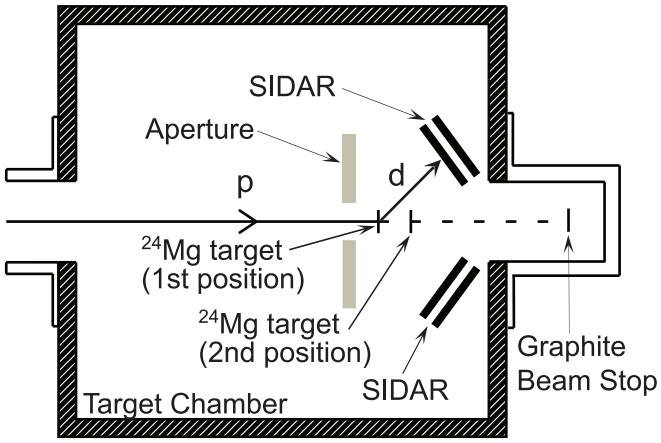

Fig. 1. Schematic diagram (not to scale) of experimental setup.

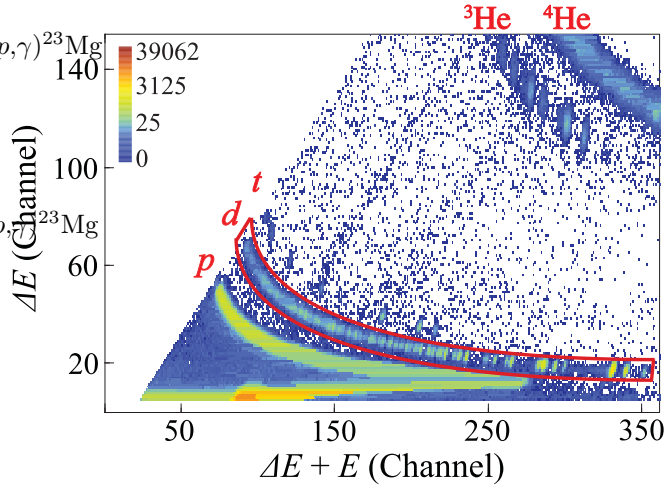

Fig. 2. (Color online) Particle identification plot of the ^{24}Mg(p,d)^{23}Mg reaction obtained at $\theta_{\rm lab}$ = 31° is shown. Charged particles such as protons, deuterons, tritons, ^{3}He, and ^{4}He are well separated. Events falling in the red gate are identified as deuterons.

2 Experimental setup

The ^{24}Mg(p,d)^{23}Mg reaction was studied by using a beam of 31 MeV protons at an intensity of ∼ 60 picoampare. The beam was delivered from the Holifield Radioactive Ion Beam Facility (HRIBF) at Oak Ridge National Laboratory (ORNL). The beam bombarded isotopically enriched (> 99.9%) ^{24}Mg solid targets located at one of two different target positions in order to cover a wide angular range of ejected particles in the silicon detectors. Target areal densities of ∼ 520 μg/cm^2 were used.

A schematic diagram of the experimental setup is shown in Fig. 1. Deuterons from the ^{24}Mg(p,d)^{23}Mg reaction (ground state Q value of −14.307 MeV) were detected using a large-area SIlicon Detector ARray (SIDAR [20]) at forward angles. The SIDAR was configured with four ΔE-E telescopes with 100-μm energy loss (ΔE) detectors backed by 1000-μm residual energy (E) detectors. Each SIDAR detector element is segmented into 16 annular strips. The angles covered by SIDAR were 16.8° ≤ $\theta_{\rm lab}$ ≤ 44.8° (18.2° ≤ $\theta_{\rm c.m.}$ ≤ 48.2°) for the first target position and 24.3° ≤ $\theta_{\rm lab}$ ≤ 63.2° (26.3° ≤ $\theta_{\rm c.m.}$ ≤ 67.6°) for the second. In order to protect the fragile silicon detectors from the intense proton beam, a thick (9.5 mm) aluminum plate with a 19 mm diameter hole was placed just in front of the target ladder. The angles and solid angles subtended by each strip were calculated using the known detector geometry. The solid angles were also measured with a calibrated ^{244}Cm α-emitting source. The measured solid angles agreed with geometrical calculations within 3%. The energy response of each strip was calibrated using another α-emitting source composed of ^{239}Pu (5.157 MeV), ^{241}Am (5.486 MeV), and ^{244}Cm (5.805 MeV). Energy resolutions were measured to be about 1% for the α particles. The energy calibration measurements were performed before and after the in-beam measurements in order to correct for any gain shifts in each strip. No significant changes were observed by comparing the calibrations. A thick graphite beam stop was placed downstream of the target chamber for monitoring beam current.

3 Excitation energy measurements

A typical particle identification plot obtained from the ΔE-E detector telescope is shown in Fig. 2. Light charged particles such as protons, deuterons, tritons, ^{3}He, and ^{4}He were identified and clearly separated by standard energy-loss techniques as shown in the figure for $\theta_{\rm lab} = 31^\circ$ ($\theta_{\rm c.m.} = 33.5^\circ$). The deuteron energies were reconstructed by summing the energies deposited in the ΔE and E layers of the silicon detectors for the events falling in the deuteron gate of the figure. The total energy of deuterons was then converted into an excitation energy in ^{23}Mg using relativistic kinematics. One example obtained at $\theta_{\rm lab} = 25.4^\circ$ is shown in Fig. 3. Thirty six peaks are labeled with their excitation energies in ^{23}Mg extracted from the current work by assuming that each peak arises from a single state. Four peaks that originated from ^{12}C and ^{16}O contamination in the targets are also labeled in the figure. The energy resolution of the peak that corresponds to the ground state was measured to be about 0.4%.

Internal energy calibrations were performed at each strip using six strongly populated and well-known energy levels: the ground state, and excited states at $E_x = 2359.0\pm1.4$, 2771±1, 5286±1, 5992±1 and 9642±8 keV [21,22]. The use of such an internal calibration minimizes the effects of most systematic uncertainties. The excitation energies in ^{23}Mg for observed levels were calculated by taking the average values of extracted energies obtained at all 16 angles. Since the reaction was measured at 16 angles simultaneously, the statistical uncertainty for the excitation energy of the level could be calculated from the standard deviation of extracted excitation energies at each angle. Excitation energies and their uncertainties obtained from the present work for 37 levels are summarized in Table 1. As shown in the table, the internal calibrations resulted in very good agreement between the excitation energies obtained from the present work and those from the recent compilation [21].

4 Spin assignments

Differential cross sections of each populated level in the center of mass system at each angle were calculated using

$$\left(\frac{d\sigma}{d\Omega}\right)_{r,\theta} = \frac{Y_{r,\theta}}{IN\Delta\Omega_\theta}, \quad (1)$$

where $Y_{r,\theta}$ is the yield of deuterons for an energy level r, I is the number of protons incident on the target, N is the number of target atoms per unit area, and $\Delta\Omega_\theta$ is the solid angle subtended by a strip of SIDAR at the angle θ.

Angular distributions extracted from the present work for six well-known low-lying energy levels ($E_x = 0.0$, 0.450, 2.771, 2.919, 3.810, and 4.363 MeV) are plotted in Fig. 4. Black (red) open circles represent the data points obtained at the first (second) target position. Statistical uncertainties are also included but are not noticeable because the uncertainties are smaller than the size of data points in most cases. Due to the uncertainties in beam current normalization and target stoichiometry, our differential cross sections are not absolute. This does not affect the shape of the angular distributions, since deuterons were measured at all angles simultaneously with each target position. To compare extracted angular distributions with theoretical calculations, distorted wave born approximation (DWBA) calculations were performed by using the zero range computer code DWUCK4 [23] with previously determined optical model parameters [16]. The results of the DWBA calculations that best fit the observed angular distributions are also included in Fig. 4 as blue solid lines. As shown in the figure, the well-known l transfers of the six low-lying energy levels can be well reproduced by the DWBA calculations. Although not shown in Fig. 4, spin assignments for many other known energy levels were well reproduced as summarized in Table 1.

As shown in the figure, the DWBA calculations provide good fits to the well-known states with $l = 0$ ($E_x = 4.363$ MeV) and $l = 2$ (ground state, $E_x = 0.450$ and 2.919 MeV). The peak at 3810±4 keV do not match to any known energy levels in ^{23}Mg. The experimental angular distribution of the peak was not characteristic of any particular l-transfer. However, when the combination of $l = 1$ (83.7%) and $l = 2$ (16.3%) was considered, the angular distribution could be well reproduced. Since there is a well-known $3/2^-$ level at $E_x = 3.793$ MeV and a ($3/2^+$, $5/2^+$) level at $E_x = 3.859$ MeV, the 3.810 MeV peak is a mixture of the two levels most likely.

The angular distribution of the peak at 2.771 MeV could not be reproduced satisfactorily as well by considering a single l-transfer. Similarly to the case of the peak at 3.810 MeV, the contribution from the well-known 2.715 MeV could affect the distribution. The combinations of two l-transfers could not be considered in this case, however, since the spin of the 2.715 MeV is known to be $9/2^+$, which corresponds to $l = 4$ in the present work. In order to consider contribution from a non-direct reaction, a constant contribution was added to the DWBA calculations, which results in better fit as shown in Fig. 4.

Angular distributions for six strongly populated high-lying states were extracted in order to constrain the spins and parities of the energy levels. Extracted angular distributions were then compared with DWBA calculations using the same set of optical model parameters described above. Only the three lowest possible l-transfers (i.e. $l =$ 0, 1, and 2) were considered, and the normalization factors were varied to best fit the experimental angular distributions. Higher l-transfers were improbable since they require unlikely configurations of nucleons in the ^{24}Mg ground state. In order to populate a ^{23}Mg state with $J^\pi = 7/2^+$, for example, there needs to be some admixture in the ^{24}Mg ground state consisting of a pair of neutrons in the $g_{7/2}$ shell, which is highly unlikely. Since such transitions via a one-step process would be extremely weak, $l =$ 4 transfers were not included for the DWBA calculations.

The 2.048 MeV state, which is well-known to be $J^\pi = 7/2^+$, is populated in the present work as shown in Fig. 3. The angular distribution of the state is, however,

Table 1. Excitation energies and spin values for levels in ^{23}Mg obtained from the present work and from the previous work are summarized. The values of previous work are taken from the compliation of Ref. [21] unless noted otherwise. All energies are in keV.

E_x Previous work	E_x This work	J^π Previous work	J^π This work	E_x Previous work	E_x This work	J^π Previous work	J^π This work
0	0[a]	$3/2^+$	$(3/2^+,5/2^+)$	7586 ± 2		$5/2^+$	
450.71 ± 0.15	450 ± 1	$5/2^+$	$(3/2^+,5/2^+)$	7624.4 ± 0.9	7625 ± 9	$(9/2)^+$	
2052.2 ± 0.9	2048 ± 2	$7/2^+$		7650[b]		$(3/2)^+$	
2359.0 ± 1.4	2359[a]	$1/2^+$		7770.2 ± 1.4		$(9/2)^+$	
2714.7 ± 1		$9/2^+$[b]		7780[b]		$(11/2)^+$	
2771 ± 3	2771[a]	$1/2^-$	$(1/2^-,3/2^-)$	7784.7 ± 1.2[d]	7788 ± 5	$(7/2)^+$	$(3/2^+,5/2^+)$
2908.1 ± 2	2919 ± 6	$3/2^+$[b]	$(3/2^+,5/2^+)$	7802.2 ± 1.4		$5/2^+$	
3793[b]		$3/2^-$		7856.1 ± 1.2[d]	7857 ± 10	$(7/2)^+$	
	3810 ± 4			8015.3 ± 0.8[d]		$(5/2,11/2)$[b]	
3859[b]		$(3/2,5/2)^+$			8044 ± 4		
3970[b]	3974 ± 3	$5/2^-$		8059 ± 2			
4353 ± 6	4363 ± 2	$1/2^+$	$1/2^+$	8076 ± 8			
4680[b]	4686 ± 7	$7/2^+$[b]		8163.9 ± 0.8[d]		$5/2^+$	
5286[b]	5286[a]	$5/2^+$[b]	$(3/2^+,5/2^+)$		8170 ± 4		
5453.2 ± 1.6	5461 ± 7	$(11/2)^+$[b]		8193 ± 8			
5656 ± 7		$5/2^+$		8287 ± 3			
5689[b]	5688 ± 7	$(1/2$ to $9/2)^+$			8330 ± 6		$(3/2^+,5/2^+)$
5711 ± 8		$(1/2$ to $9/2)^+$		8342 ± 2[c]			
5936[b]				8393 ± 6			
5992[b]	5992[a]	$(1/2,3/2)^-$		8420 ± 6			
6128[b]	6144 ± 3	$(7/2)^-$[b]	$(3/2^+,5/2^+)$		8436 ± 7		
6192[b]		$(13/2)^+$		8453 ± 5		$3/2^+,5/2^+,7/2^+$	
6238[b]	6246 ± 4	$(1/2$ to $9/2)^+$		8557 ± 6			
6371[b]	6391 ± 2	$(7/2)^+$[b]	$(3/2^+,5/2^+)$	8617 ± 6			
6448[b]		$(9/2)^-$[b]		8758 ± 6	8770 ± 8		
6512[b]		$(7/2)^+$[b]		8793 ± 8			
6538 ± 5	6537 ± 3	$(1/2$ to $9/2)^+$	$(3/2^+,5/2^+)$	8870 ± 8			
6573[b]		$5/2^+$		8916 ± 6	8924 ± 5		
6774[b]		$(1/2,5/2)$[b]		8943 ± 7		$(15/2)^+$	
6802[b]	6802 ± 2	$(5/2)^-$[b]	$(3/2^+,5/2^+)$	8990 ± 6		$(1/2$ to $9/2)^+$	
6810 ± 6				9018 ± 6			
6899 ± 5	6912 ± 6	$5/2^+$	$(3/2^+,5/2^+)$	9060 ± 8			
6984 ± 5		$5/2^+$		9103 ± 6			
	7007 ± 5		$(3/2^+,5/2^+)$		9123 ± 7		
7020[b]		$(1/2$ to $9/2)^+$		9138 ± 6			
7110[b]				9253 ± 8			
7143[b]	7144 ± 4	$(5/2)^+$	$(3/2^+,5/2^+)$	9328 ± 8	9350 ± 13		
7227[b]				9374 ± 8			
7260[b]	7260 ± 6		$(3/2^+,5/2^+)$	9403 ± 8			
7381 ± 8				9420 ± 8			
7449[b]	7441 ± 8			9465 ± 6	9472 ± 7	$(1/2$ to $9/2)^+$	
7495[b]				9596 ± 7		$(17/2)^+$	
				9642 ± 8	9642[a]		

[a] This energy level is used for the internal energy calibration.
[b] Taken from Ref. [22]. Energy uncertainty of this level is measured to be about ±1 keV.
[c] Taken from Ref. [10].
[d] Taken from Ref. [2].

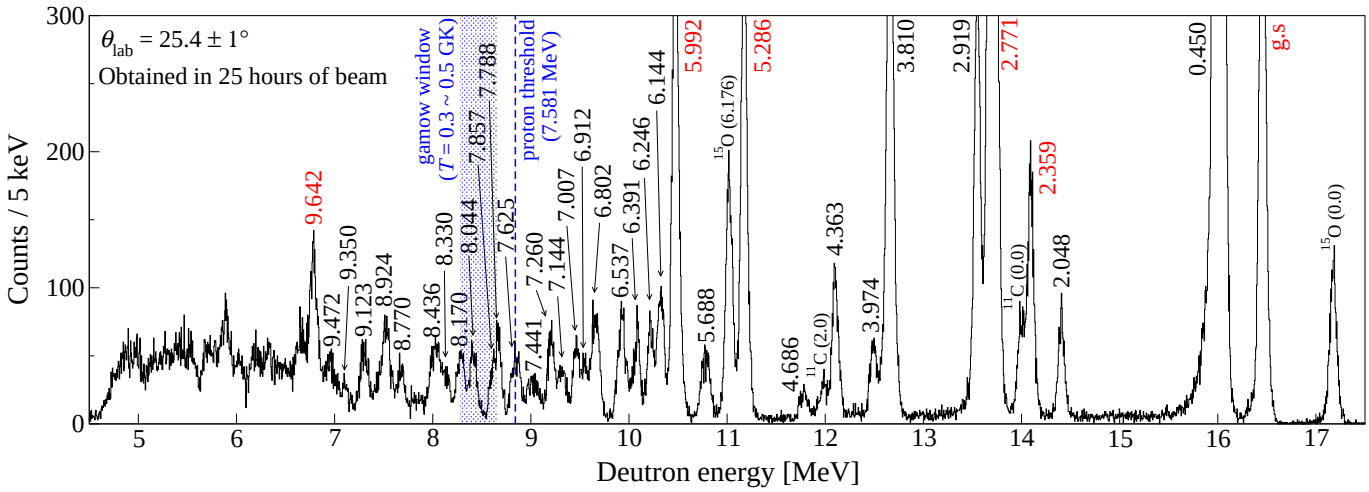

Fig. 3. (Color online) A typical energy spectrum for the deuterons gated on the ΔE-E spectrum is shown. The spectrum is obtained at $\theta_{\rm lab} = 25.4^{\circ}$ in this case. Energy levels used for internal energy calibrations are labeled in red (see text). All excitation energies are shown in MeV. Four peaks originated from the ^{12}C and ^{16}O contaminations in the targets are also labeled. The blue shaded area represents the Gamow window calculated for the ^{22}Na + p system at the typical nova temperature range of $T = 0.3$–0.5 GK.

not characteristic of a single step process, and cannot be reproduced by the DWBA calculations as shown in Fig. 5. In such a case, considering a two-step process which involves the excitation of ^{24}Mg nucleus and the nucleon pickup could give a satisfactory explanation.

In Fig. 6, the empirical angular distributions and results of DWBA calculations for $l = 0$, 1, and 2 transfers for six energy levels are shown: $E_x = 6.144$, 6.391, 6.802, 7.260, 7.788, and 8.330 MeV. As shown in the figure, $l = 2$ transfers best fit the experimental data for the levels, which corresponds to $J^{\pi} = 3/2^{+}$ or $5/2^{+}$. The spins of the states at $E_x = 7.260$ and 8.330 MeV have not been reported so far. Excitation energies and spin assignments of ^{23}Mg levels extracted from the present work assume that each peak arose from a singlet state.

Spin assignments for ^{23}Mg levels in the present work show good agreement with the previous works except for the $E_x = 6.144$, 6.391, 6.802, and 7.788 MeV states as summarized in Table 1. Spins of the $E_x = 6.144$, 6.391, and 6.802 MeV levels were constrained only through the γ-ray spectroscopic study using the ^{12}C(^{12}C,n)^{23}Mg reaction performed by Jenkins *et al.* [22]. The Directional Correlations of γ-rays deexciting Oriented states ratios ($R_{\rm DCO}$) from each decay was measured by the Gammasphere array [24] to constrain the spins and parities for the $E_x = 6.144$ and 6.391 MeV levels. For example, the $R_{\rm DCO}$ values of the decay from 6.144 MeV level to 3.974 MeV level ($J^{\pi} = 5/2^{-}$) was determined to be 1.28 ± 0.09. The $R_{\rm DCO}$ values should be close to 0.9 ± 0.1 for pure stretched-dipole transitions and 1.8 ± 0.1 for pure stretched-quadrupole transitions in their detector geometry. Although the decay was identified as the $M1/E2$ transition, the spin of the 6.144 MeV level was assigned to be $7/2^{-}$ in the reference. In the case of a mixed transition, therefore, constraining the spin and parity of a state through the angular correlation measurement in conjunction with the observed branching in the decay of the state to a well-known energy level is not always straightforward [25].

5 The 7.788 MeV level: dominant resonance for ^{22}Na(p,γ)^{23}Mg reaction rate

Since the energy level at $E_x = 7.788$ MeV is believed to be a dominant resonance state for the ^{22}Na(p,γ)^{23}Mg reaction rate at stellar temperatures, the spin of the state has been a subject of many theoretical and experimental studies [22,26–29]. In the γ-ray spectroscopic study mentioned above, the level was observed to decay to the 0.450 MeV level ($J^{\pi} = 5/2^{+}$) by $M1/E2$ transition [22]. In accordance with the discussion of the previous section, the authors assigned $J^{\pi} = 7/2^{+}$ for the level by using the measured $R_{\rm DCO}$ value of 0.89 ± 0.05 and the branching in the decay to the well-known 0.450 MeV level. The assignment is, however, not definite without knowing the mixing ratio.

In the β-delayed proton decay study of ^{23}Al performed by Saastamoinen *et al.* [26], no strong isospin mixing was observed for the 7.788 and 7.802 MeV levels. The authors argued that the spin of the 7.788 MeV state could not be $5/2^{+}$, since the 7.802 MeV level ($J^{\pi} = 5/2^{+}$) was identified as the isobaric analogue state (IAS) of the ground state of ^{23}Al. Although the presence of isospin mixing can constrain spin and parity, the absence of the mixing cannot. Moreover, this result contradicts that of Tighe *et al.* [30], where extremely strong isospin mixing of the IAS in ^{23}Mg was observed.

In more recent work by Tripathi *et al.* [29], shell model calculations using the USDA interaction in the *sd* shell were performed to try to reproduce a $J^{\pi} = 7/2^{+}$, $T = 1/2$ state at the 7.788 MeV. Such a state, however, could not

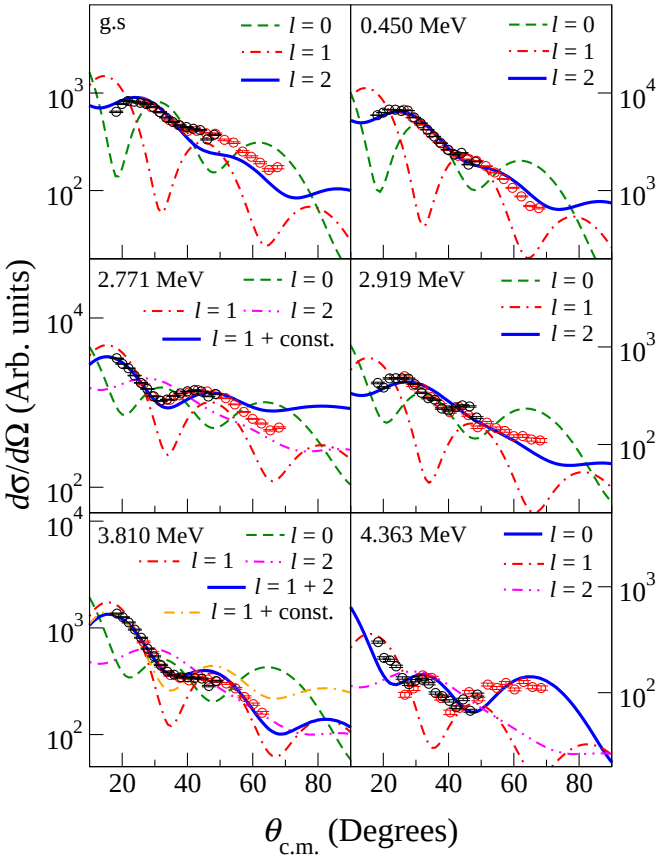

Fig. 4. (Color online) Angular distributions of deuterons from the ^{24}Mg$(p,d)^{23}$Mg reaction for six well-known low-lying energy levels are shown. Black (red) open circles represent the data points obtained at the first (second) target position. The results of DWBA calculations for l = 0, 1, and 2 transfers are also shown. DWBA calculations best fitting the observed angular distributions are shown as blue solid lines.

be predicted, but a $J^\pi = 5/2^+$ state was predicted with a very small $B(GT)$ value. Therefore, it was suggested that the 7.802 and 7.788 MeV states in ^{23}Mg represent a split IAS with $J^\pi = 5/2^+$.

In the present work, the observed angular distribution of deuterons obtained from the 7.788 MeV level is best fit with an $l = 2$ transfer as shown in Fig. 6. When a direct, one-step reaction is assumed, the result indicates that a neutron was picked-up from the $1d$ shell in the ^{24}Mg ground state, which implies that the spin should be $3/2^+$ or $5/2^+$. Since the β-delayed proton emission was observed for the level [26], $J^\pi = 3/2^+$ is ruled-out. Therefore, $J^\pi = 5/2^+$ was used for the ^{22}Na$(p,\gamma)^{23}$Mg reaction rate calculation. Due to the discrepancy in the previous β-delayed proton decay studies [26,30] and the result from a recent γ-ray spectroscopy study [22], we adopt a conservative approach to address this uncertainty in the literature by considering $J^\pi = 7/2^+$ as well for the reaction rate calculation.

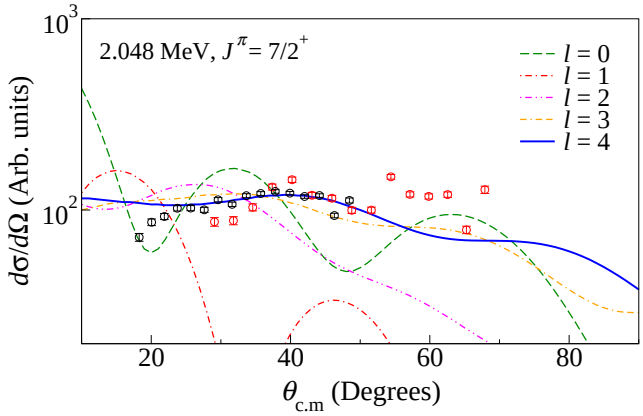

Fig. 5. (Color online) Experimental angular distribution of deutrons from the ^{24}Mg$(p,d)^{23}$Mg reaction for the E_x = 2.048 MeV ($J^\pi = 7/2^+$) level. The results of DWBA calculation for l = 0, 1, 2, 3, and 4 transfers are also shown.

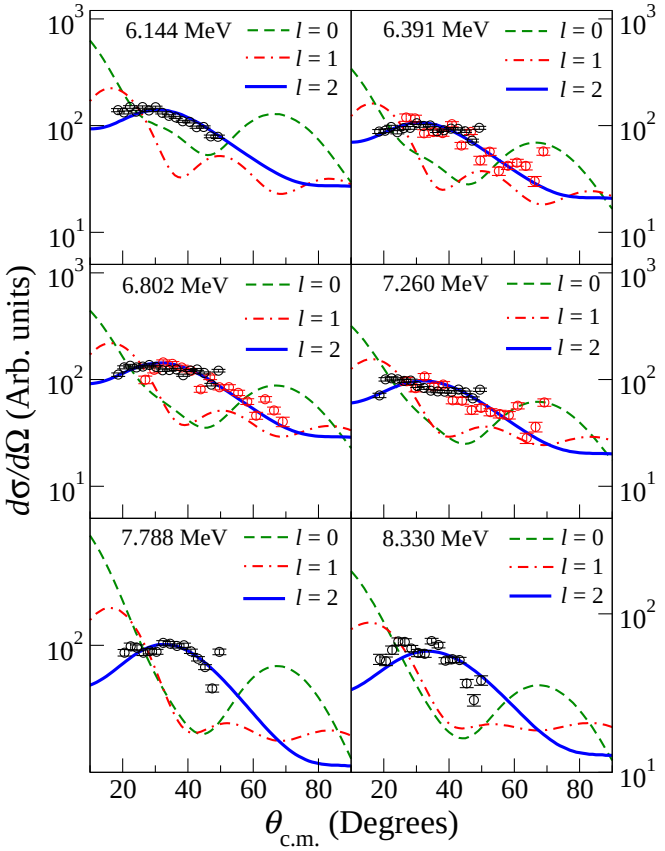

Fig. 6. (Color online) Experimental angular distributions of deuterons from the ^{24}Mg$(p,d)^{23}$Mg reaction (black and red circles) and DWBA calculations best fitting the experimental data (solid lines) are shown for six energy levels.

6 Reaction rate calculation

The ^{22}Na$(p,\gamma)^{23}$Mg reaction rate at nova temperatures was calculated using the narrow resonance formalism:

$$N_A \langle \sigma v \rangle = \frac{1.5399 \times 10^{11}}{\left(\frac{M_p M_{^{22}\mathrm{Na}}}{M_p + M_{^{22}\mathrm{Na}}} T_9\right)^{3/2}} \times \sum_i (\omega\gamma)_i e^{-11.605 E_i / T_9} \left[\mathrm{cm^3 mol^{-1} s^{-1}}\right], \quad (2)$$

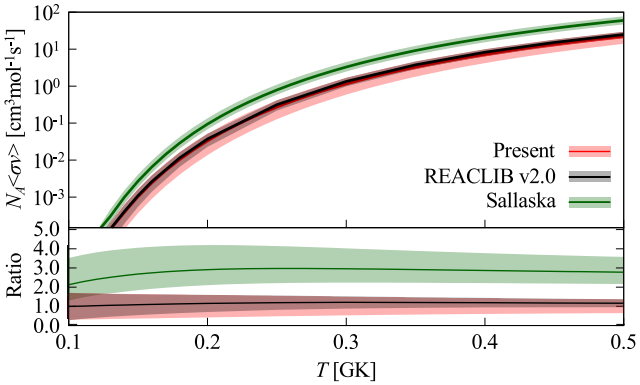

Fig. 7. (Color online) (top) The ^{22}Na(p,γ)^{23}Mg reaction rate calculated through the present work is shown. The reaction rates adopted by Sallaska *et al.* and the REACLIB v2.0 library are also shown. (bottom) The ratios between the present rate and the previous rates are shown.

where i is the index of the resonance, M is the atomic mass of subscripted particle, $\omega\gamma$ is the resonance strength in MeV, E is the resonance energy, and T_9 is temperature in GK. Resonance parameters used in the reaction rate calculation are summarized in Table 2. Twelve levels above the proton threshold located at 7.581 MeV were included in the reaction rate calculation. The calculated ^{22}Na(p,γ)^{23}Mg reaction rate as a function of temperature is plotted in the top panel of Fig. 7.

The ^{22}Na(p,γ)^{23}Mg reaction rate compiled in the REACLIB v2.0 library [32] was calculated by Iliadis *et al.* [33], where the resonance strength of the 7.788 MeV level was estimated to be 1.4 ± 0.3 meV by using the experimental yield of Stegmüller *et al.* [11] and the measured branching ratio of Jenkins *et al.* [22]. The reaction rates adopted by Sallaska *et al.* [2] and the REACLIB v2.0 library are also shown in the top panel of Fig. 7 for comparison.

For the present ^{22}Na(p,γ)^{23}Mg reaction rate calculation, spin value of ($5/2^+$, $7/2^+$) was used as explained in the previous section. The resonance strength value for $J^\pi = 7/2^+$ was adopted from recent indirect study by Saastamoinen *et al.* ($\omega\gamma = 1.4^{+0.5}_{-0.4}$ meV, [26]), which was derived from a lifetime and branching ratio measurement. Since the resonance strength $\omega\gamma$ is proportional to $(2J + 1)$, where J is the spin of the resonance, changing the spin value from $7/2^+$ to $5/2^+$ would cause a factor of 3/4 reduction in the resonance strength. Therefore, $\omega\gamma = 1.05^{+0.375}_{-0.3}$ meV was used for $J^\pi = 5/2^+$. Since the value of resonance strength ranges from 0.75 to 1.9 meV when both $J^\pi = 7/2^+$ and $5/2^+$ are considered, $\omega\gamma = 1.325 \pm 0.575$ meV was used as a result, which overlaps with the limits suggested by Iliadis *et al.* and Saastamoinen *et al.* The value is, however, more than a factor of four smaller than that of Sallaska *et al.*

The ^{22}Na(p,γ)^{23}Mg reaction rate from the present work is about a factor of three smaller than the rate of Sallaska *et al.* and about 21% smaller than the current "standard" rate found in the REACLIB v2.0 library at $T = 0.3$ GK. In the bottom panel of Fig. 7, the reaction rate ratio $N_A < \sigma v >_{\rm REACLIB}/N_A < \sigma v >_{\rm present}$($N_A < \sigma v >_{\rm Sallaska}/N_A < \sigma v >_{\rm present}$) is shown as a black (green) solid line. The shaded areas represent the uncertainties in the ratios. The total reaction rate shown in the figure is a sum of contributions from 12 levels. Since there may be missing or unresolved levels not accounted for by the current reaction rate calculation, our total reaction rate can be considered to be a lower limit for the rate.

7 Astrophysical implications

In order to explore how the new ^{22}Na(p,γ)^{23}Mg reaction rate affects the final abundance of ^{22}Na during nova explosions, element synthesis calculations were performed in the framework employed in the Computational Infrastructure for Nuclear Astrophysics (CINA) [34]. CINA uses a nuclear reaction network containing 422 isotopes from ^{1}H to ^{82}Se with nuclear reaction rates from the REACLIB v2.0 database. The ejected envelope of a nova outburst is divided into 23 zones in the calculation and the thermodynamic history of each zone is considered for 1.15 $M_\odot$, 1.25 $M_\odot$, and 1.35 $M_\odot$ ONeMg white dwarfs [35]. Reaction network calculations were performed at each zone independently, and the final abundance of ^{22}Na was determined by a sum of each zone's ^{22}Na contribution weighted by the ratio of the zone mass to the total envelope mass for each mass of white dwarf.

The final weighted abundance of ^{22}Na was calculated using the reaction rates of the REACLIB v2.0 data base first and comparing with the calculated abundance using the updated library (i.e. the reaction rate library based on the REACLIB v2.0 with our ^{22}Na(p,γ)^{23}Mg reaction rate.) The results are summarized in Fig. 8. A similar calculation was also performed by using the REACLIB library with the ^{22}Na(p,γ)^{23}Mg reaction rate of Sallaska *et al.* and the results are summarized in the figure as well. The lower and the upper limits in the final ^{22}Na abundances, result from the highest and the lowest ^{22}Na(p,γ)^{23}Mg reaction rates used in the library, respectively. The calculations indicate that the ^{22}Na final abundance, predicted using the present rate of 5.7×10^{-9} $M_\odot$, is 42% (5%) higher than that of using the ^{22}Na(p,γ)^{23}Mg reaction rate of Sallaska *et al.* (REACLIB library) for a 1.35 $M_\odot$ ONeMg white dwarf. The present value of the final abundance is close to the values deduced from previous works: 2.9×10^{-8} $M_\odot$ by Starrfield *et al.* [36], 2.2×10^{-9} $M_\odot$ by José *et al.* [37], and 1.9×10^{-9} $M_\odot$ by Sallaska *et al.* [2].

The 1.275 MeV γ-ray emission from the decay of ^{22}Na has been searched by using the Imaging Compton Telescope (COMPTEL). Although no evidence could be found for the 1.275 MeV γ-ray detection, the 2σ upper limits to the ejected ^{22}Na mass for neon-type novae could be derived to be 3.7×10^{-8} $M_\odot$ by using background analysis of the ^{22}Na line flux [12]. The upper limit on the final ^{22}Na abundance deduced from the present work is about a factor of five less than that of the observational upper limit. By using the modern detection systems on a space-based telescope such as the spectrometer on INTEGRAL

Table 2. Resonance parameters used for the ^{22}Na(p,γ)^{23}Mg reaction rate calculation are summarized.

E_x [keV]	E_r [keV]	J^π	$\omega\gamma$ [meV]
7586 ± 2[a]	5 ± 2	$5/2^{+}$[a]	3.6×10^{-33}[b]
7624.4 ± 0.9[a]	43.4 ± 0.9	$9/2^{+}$[a]	1.14×10^{-12}[c]
7648 ± 3[a]	67 ± 3	$3/2^{+}$[a]	4.57×10^{-9}[c]
7770.2 ± 1.4[a]	189.2 ± 1.4	$9/2^{+}$[a]	$0.34^{+0.25}_{-0.22}$[e]
7784.7 ± 1.2[e]	203.7 ± 1.2	($7/2^{+}$[a], $5/2^{+}$[d])	1.325 ± 0.575[f]
7856.1 ± 1[e]	275.1 ± 1	$7/2^{+}$[a]	15.8 ± 3.4[e]
8015.3 ± 0.8[e]	434.3 ± 0.8		68 ± 20[e]
8059 ± 2[a]	478 ± 2		37 ± 12[e]
8163.9 ± 0.8[e]	582.9 ± 0.8	$5/2^{+}$[a]	235 ± 33[e]
8287 ± 3[a]	706 ± 3		364 ± 60[e]
8330 ± 10[d]	749 ± 10	$3/2^{+}$[d]	95 ± 30[e]
8924 ± 6[d]	1343 ± 6	$5/2^{+}$[b]	830[b]

[a] From Ref. [21].
[b] Taken from theoretical predictions [28,31].
[c] Derived from theoretical prediction [28].
[d] This work.
[e] Taken from direct measurements [2,11,10].
[f] Derived from lifetime measurement [26].

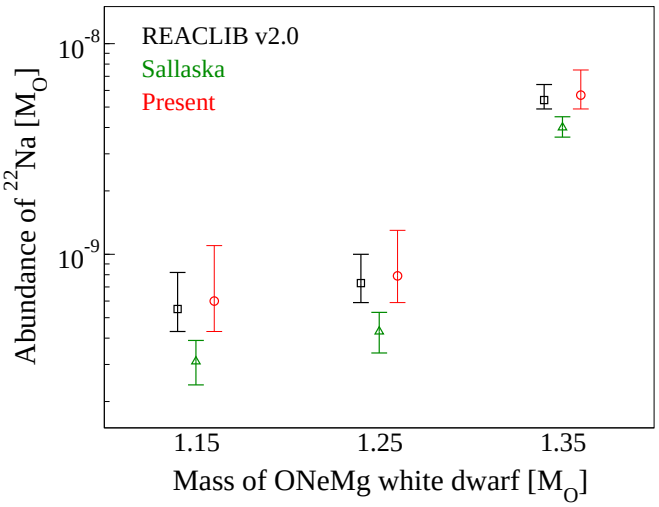

Fig. 8. (Color online) Final weighted abundance of ^{22}Na calculated by using three reaction rate libraries for three different masses of ONeMg white dwarfs are shown.

(SPI), for instance, significant constraints on nova nucleosynthesis could be obtained for a nova less than 0.5 kpc away with an observation time of more than 10^6 seconds by considering the sensitivity of SPI for the ^{22}Na line ($\sim$3 $\times$ 10^{-5} photons·cm^{-2}·s^{-1}) [1]. When more advanced spectrometer such as ACT is available in the future with much better sensitivity of about 3 $\times$ 10^{-7} photons·cm^{-2}·s^{-1} [1, 3], nova events occurring near the center of the galaxy might be detectable.

8 Conclusion

The ^{24}Mg(p,d)^{23}Mg reaction was studied at the ORNL HRIBF to improve our understanding of the astrophysically-important ^{22}Na(p,γ)^{23}Mg reaction. The energies and angular distributions of the deuterons from the ^{24}Mg(p,d)^{23}Mg reaction were measured at several angles simultaneously by using an annular silicon detector array. By comparing the observed angular distributions with DWBA calculations, the following spin and parity assignments were constrained: E_x = 7.788 MeV ($3/2^+$, $5/2^+$), E_x = 7.260 MeV ($3/2^+$, $5/2^+$), and E_x = 8.330 MeV ($3/2^+$, $5/2^+$).

To study the effect of the newly suggested spin on the ^{22}Na(p,γ)^{23}Mg reaction rate, the resonance parameters were updated from the previous work [2,10,11,26,28, 31]. The calculation shows that our resulting reaction rate is about a factor of three smaller than that of recent work by Sallaska *et al.* [2] at T = 0.3 GK. Using the updated reaction rate, we have investigated the final abundances of the radionuclide ^{22}Na produced in a nova nucleosynthesis model for a 1.35 $M_\odot$ ONeMg white dwarf. The result shows that the final weighted ^{22}Na abundance calculated using the newly constrained reaction rate is determined to be about 42% higher than that of using the ^{22}Na(p,γ)^{23}Mg reaction rate of Sallaska *et al.* When compared with the final abundance calculated by using standard rate found in the REACLIB v2.0 library, our abundance is about 5% higher. The ^{22}Na abundance calculated from the present work will be compared with the future observational results from SPI of INTEGRAL or more advanced future spectrometers such as ACT and e-ASTROGAM.

9 Acknowledgements

This work was supported by a National Research Foundation of Korea (NRF) grant funded by the Korea government Ministry of Education, Science, and Technology (MEST) Nos. NRF-2013M7A1A1075764, NRF-2016R1A5A1013277, and NRF-2019R1F1A1058370. This research was supported in part by the National Nuclear Security Administration under the Stewardship Science Academic Alliances program through the U.S.DOE Cooperative Agreement No. DE-FG52-08NA285
52 with Rutgers University and Oak Ridge Associated Universities. This work was also supported in part by the Office of Nuclear Physics, Office of Science of the U.S.DOE under Contracts No. DE-FG02-96ER40955 with Tennessee Technological University, No. DE-FG02-96ER40983 with the University of Tennessee, and DE-AC-05-00OR22725 at Oak Ridge National Laboratory, and by the National Science Foundation under Contract No. PHY-1713857 with University of Notre Dame.

References

1. M. Hernanz and J. José, New Astron. Rev. **48**, (2004) 35.
2. A. L. Sallaska *et al.*, Phys. Rev. C **83**, (2011) 034611.
3. S. E. Boggs, New Astron. Rev. **50**, (2006) 604.
4. A. De Angelis *et al.*, J. High Energy Astrophysics **19**, (2018) 1.
5. D. D. Clayton and F. Hoyle, Astrophys. J. **187**, (1974) L101.
6. J. José, A. Coc, and M. Hernanz, Astrophys. J. **520**, (1999) 347.
7. C. Iliadis, A. Champagne, J. José, S. Starrfield, and P. Tupper, Astrophys. J. Suppl. Ser. **142**, (2002) 105.
8. W. R. Hix, M. S. Smith, S. Starrfield, A. Mezzacappa, and D. L. Smith, Nucl. Phys. A **718**, (2003) 620.
9. M. Wang, G. Audi, F. G. Kondev, W. J. Huang, S. Naimi, and X. Xu, Chin. Phys. C **41**, (2017) 030003.
10. S. Seuthe, C. Rolfs, U. Schröder, W. H. Schulte, E. Somorjai, H. P. Trautvetter, and F. B. Waanders, Nucl. Phys. A **514**, (1990) 471.
11. F. Stegmüller, C. Rolfs, S. Schmidt, W. H. Schulte, H. P. Trautvetter, and R. W. Kavanagh, Nucl. Phys. A **601**, (1996) 168.
12. A. F. Iyudin *et al.*, Astron. Astrophys. **300**, (1995) 422.
13. L. C. Haun and N. R. Roberson, Nucl. Phys. A **140**, (1970) 333.
14. H. Nann, A. Saha, and B. H. Wildenthal, Phys. Rev. C **23**, (1981) 606.
15. S. Schmidt, C. Rolfs, W. H. Schulte, H. P. Trautvetter, R. W. Kavanagh, C. Hategan, S. Faber, B. D. Valnion, and G. Graw, Nucl. Phys. A **591**, (1995) 227.
16. R. L. Kozub, Phys. Rev. **172**, (1968) 1078.
17. J. Källne and B. Fagerström, Phys. Scr. **11**, (1975) 79.
18. D. W. Miller *et al.*, Phys. Rev. C **20**, (1979) 2008.
19. S. Kubono *et al.*, Z. Phys. A **348**, (1994) 59.
20. D. W. Bardayan *et al.*, Phys. Rev. C **63**, (2001) 065802.
21. R. B. Firestone, Nuclear Data Sheets **108**, (2007) 1.
22. D. G. Jenkins *et al.*, Phys. Rev. C **87**, (2013) 064301.
23. P. D. Kunz, http://spot.colorado.edu/∼kunz/ (unpublished).
24. I. Y. Lee, Nucl. Phys. A **520**, (1990) 641c.
25. A. Krämer-Flecken, T. Morek, R. M. Lieder ,W. Gast, G. Hebbinghaus, H. M. Jäger, and W. Urban, Nucl. Instrum. Methods A **275**, (1989) 333.
26. A. Saastamoinen *et al.*, Phys. Rev. C **83**, (2011) 045808.
27. O. S. Kirsebom *et al.*, Phys. Rev. C **93**, (2016) 025802.
28. M. Wiescher and K. Langanke, Z. Phys. A **325**, (1986) 309.
29. V. Tripathi, S. L. Tabor, A. Volya, S. N. Liddick, P. C. Bender, N. Larson, C. Prokop, S. Suchyta, P. L. Tai, and J. M. VonMoss, Phys. Rev. Lett. **111**, (2013) 262501.
30. R. J. Tighe, J. C. Batchelder, D. M. Moltz, T. J. Ognibene, M. W. Rowe, Joseph Cerny, and B. A. Brown, Phys. Rev. C **52**, (1995) R2298.
31. S. J. Jin *et al.*, Phys. Rev. C **88**, (2013) 035801.
32. R. H. Cyburt *et al.*, Astrophys. J. Suppl. Ser. **189**, (2010) 240.
33. C. Iliadis, R. Longland, A. E. Champagne, A. Coc, and R. Fitzgerald, Nucl. Phys. A **841**, (2010) 31.
34. http://nucastrodata.org.
35. S. Starrfield, C. Iliadis, W. R. Hix, F. X. Timmes, and W. M. Sparks, Astrophys. J. **692**, (2009) 1532.
36. S. Starrfield, J. W. Truran, M. C. Wiescher, and W. M. Sparks, Mon. Not. R. Astron. Soc. **296**, (1998) 502.
37. J. José and M. Hernanz, Astrophys. J. **494**, (1998) 680.